Int. J. Heat Mass Transfer. Vol. 30, No. 5, pp. 903–909, 1987
Printed in Great Britain

0017–9310/87 $3.00 + 0.00

Adiabatic–isothermal mixed boundary conditions in heat transfer

J. L. BASSANI, M. W. NANSTEEL and M. NOVEMBER
Department of Mechanical Engineering and Applied Mechanics, University of Pennsylvania, Philadelphia, PA 19104, U.S.A.

(*Received* 1 *October* 1985 *and in final form* 8 *September* 1986)

Abstract—Mixed boundary conditions of the adiabatic–isothermal type often arise in the mathematical modeling of heat transfer phenomena. Under certain circumstances, the mixed condition gives rise to singular behavior which cannot be adequately treated by numerical means alone. The numerical procedure must be supplemented by an asymptotic analysis for the local behavior near the singularity. In the special case of a mixed boundary condition on a straight boundary, the strength of the singularity is given in terms of a path-independent integral, the value of which can be determined from the numerical solution for the far-field behavior. Implications of overlooking the singular behavior due to the mixed boundary condition are discussed.

1. INTRODUCTION

A WIDE range of problems in continuum mechanics involve mixed boundary conditions. Solutions to these problems can display singularities in flux quantities (e.g heat flux, electrostatic flux, strain, etc.) while the total energy of the system remains bounded [1, 2]. Generally, the asymptotic solution that characterizes the singular behavior dominates the complete solution in a small region of relevant dimensions in the neighborhood of the singular point. In fact, stress and strain singularities at the tip of a sharp crack form the foundation of fracture mechanics [3, 4]. The study of singularities has received less attention in heat transfer, although they naturally arise in many problems [5–11]. Through an example, it is shown that a reliable estimate of the total energy transferred in the neighborhood of a singularity, which is often the major portion of the energy of the system, requires that the singularity be carefully treated.

In this paper, steady-state temperature fields are considered in a wedge-shaped region $0 \leqslant \theta \leqslant \alpha, r \geqslant 0$ where, at the vertex of the wedge, the boundary condition changes abruptly from isothermal to adiabatic. Therefore, the vertex is a point of flux singularity. Whenever the included angle α is greater than $\pi/2$ the heat flux is unbounded at the vertex. We begin with a local eigenvalue analysis that determines the asymptotic temperature field in the neighborhood of the vertex to within a multiplicative (amplitude) factor, A_0. For some simple geometries, A_0 can be found from closed form solutions based on, e.g. dual series, singular integral equations, or conformal mapping [1, 2]. Otherwise, however, A_0 must be determined numerically.

Due to the presence of the flux singularity, it is generally difficult to determine A_0 accurately from numerical calculations alone since a finite discretization around the singularity cannot reproduce the steep gradients there. Therefore, prior knowledge of the form of the asymptotic solution is very useful, if not essential, in numerically determining A_0. This is demonstrated by finite difference solutions for the steady-state temperature field in a plate with an adiabatic–isothermal mixed-boundary condition along one edge. It is shown that when the mixed-boundary condition arises along a straight boundary, the amplitude factor A_0 can be readily determined from the temperature field far from the singularity in terms of a path-independent integral (that is analogous to the J-integral of fracture mechanics [12]). In regions remote from the singularity the numerical solutions tend to be relatively accurate, and therefore, by evaluating this integral along a path far from the singularity an accurate estimate of A_0 is obtained.

2. LOCAL ANALYSIS

2.1. *Asymptotic solution*

Consider the solid, wedge-shaped region $0 \leqslant \theta \leqslant \alpha$ with vertex angle α, in which the steady-state temperature field is governed by Laplace's equation. Due to a discontinuous change in the boundary condition at the vertex, $r = 0$, from the first kind on $\theta = 0$ to the second kind on $\theta = \alpha$, there is a flux singularity [1, 2] and the temperature field near $r = 0$ depends on remote boundary conditions only through a multiplicative constant. In this sense, therefore, the local problem is autonomous and can be investigated independent of the overall geometry surrounding the vertex.

NOMENCLATURE

A_n	coefficients in equation (2a)
A_0	strength of flux singularity
C	integration path, equation (7)
J	value of path-independent integral, equation (7)
k	thermal conductivity
M	number of grid spacings in inner grid
n	index in equation (2a)
N	number of grid spacings in outer grid
q	magnitude of heat flux, equation (6)
q_0	far-field estimate of heat flux
q_r	radial component of heat flux
q_θ	component of heat flux in θ-direction
Q_L	heat transfer across lower surface of plate
Q_U	heat transfer across upper surface of plate
Q_θ	heat transfer in θ-direction
r	radial coordinate
T	temperature
x	horizontal coordinate
x^*	matching coordinate used in two-term approximation
x_0	half-width of rectangular path
y	vertical coordinate
y_0	height of rectangular path.

Greek symbols

α	wedge angle, Fig. 1
θ	angular coordinate
λ_n	eigenvalue, equation (2b).

In the neighborhood of the vertex, with isothermal conditions along $\theta = 0$ and adiabatic conditions† along $\theta = \alpha$, the steady-state temperature distribution $T(r, \theta)$ satisfies

$$\frac{1}{r}\frac{\partial}{\partial r}\left(r\frac{\partial T}{\partial \theta}\right) + \frac{1}{r^2}\frac{\partial^2 T}{\partial \theta^2} = 0 \tag{1a}$$

$$T(r, 0) = 0, \qquad \frac{\partial T}{\partial \theta}(r, \alpha) = 0. \tag{1b, c}$$

The separable solution to equation (1a) that satisfies equations (1b) and (1c) and has a bounded temperature at $r = 0$ is

$$T(r, \theta) = \sum_{n=0}^{\infty} A_n r^{\lambda_n} \sin \lambda_n \theta, \qquad \lambda_n = \frac{(2n+1)\pi}{2\alpha}. \tag{2a, b}$$

The coefficients A_n are determined, in general, from far-field boundary conditions and not from the local analysis. If the flux singularity occurs at a point on the boundary which has finite curvature the present analysis applies with $\alpha = \pi$ since locally ($r \to 0$) the radius of curvature of the boundary will be large compared with r.

Near the vertex, the asymptotic behaviors of temperature and heat flux follow from equation (2): as $r \to 0$

$$T(r, \theta) = A_0 r^{\pi/2\alpha} \sin\left(\frac{\pi}{2\alpha}\theta\right) \tag{3}$$

$$q_r(r, \theta) = -k\frac{\partial T}{\partial r} = -A_0\left(\frac{k\pi}{2\alpha}\right) r^{\pi/2\alpha - 1} \sin\left(\frac{\pi}{2\alpha}\theta\right) \tag{4}$$

$$q_\theta(r, \theta) = \frac{-k}{r}\frac{\partial T}{\partial \theta} = -A_0\left(\frac{k\pi}{2\alpha}\right) r^{\pi/2\alpha - 1} \cos\left(\frac{\pi}{2\alpha}\theta\right) \tag{5}$$

$$q = |\nabla T| = (q_r^2 + q_\theta^2)^{1/2} = A_0\left(\frac{k\pi}{2\alpha}\right) r^{\pi/2\alpha - 1} \tag{6}$$

where k is the thermal conductivity. Equations (4) and (5) show that for wedge angles $\alpha > \pi/2$ the fluxes q_r and q_θ both exhibit a singularity at the vertex of order $r^{\pi/2\alpha - 1}$. A plot of the order of the singularity, $\pi/2\alpha - 1$, vs the wedge angle α is given in Fig. 1. For $\alpha > \pi/2$, even though the flux is unbounded at $r = 0$, the total energy flow into or out of the region around $r = 0$ is bounded.

The far-field (remote) geometry and boundary conditions enter into the asymptotic behavior only through the single multiplicative factor A_0, which is the strength of the flux singularity that appears in equations (3)–(6). By matching equation (2) to the far-field solution for a particular problem, A_0 can be determined. In general, for complex geometries and far-field boundary conditions, A_0 must be determined from numerical solutions. Whether using finite difference, finite element, boundary element, or some other numerical method, due to the flux singularity, special care in choosing a sufficiently fine discretization around $r = 0$ must be taken to accurately calculate A_0 and to interpret the numerical results [13, 14]. Generally, a tedious procedure involving mesh refinement is required to check convergence. Typical features of a numerical solution of problems involving singularities are discussed below through an example.

†In the case of a constant, non-zero flux on $\theta = \alpha$, i.e. $(\partial T/\partial\theta)(r, \alpha) = f$, equation (1) is recovered through the simple substitution $\bar{T}(r, \theta) = T(r, \theta) - f\theta$.

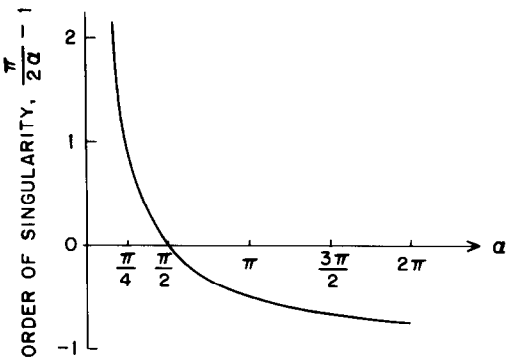

FIG. 1. Order of flux singularity as a function of wedge angle, α.

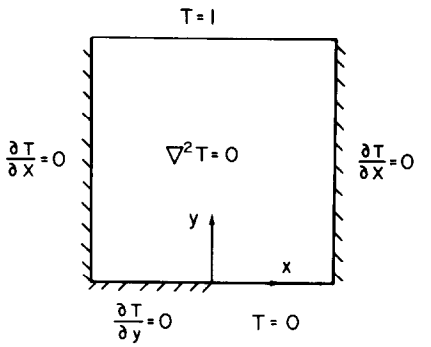

FIG. 2. Steady heat conduction in a square plate with a flux singularity at $x = y = 0$.

2.2. A_0 *via the J-integral*

When $\alpha = \pi$ the thermal problem considered here resembles a problem in fracture mechanics† for which Rice [12] has shown that A_0 is directly related to a path-independent integral that is evaluated along any path from $\theta = 0$ to π. This fact has greatly aided both the analytical and experimental determination of A_0 in the study of fracture [16]. The mixed-boundary-value problem associated with $\alpha = \pi$ arises in a number of contexts in heat transfer. Examples are the surface rewetting problem in loss-of-coolant accident studies [6], contact resistance problems [7], enclosure convection [9] and heat loss from buried pipes [5].

Consider the half-space $r > 0, 0 \leqslant \theta \leqslant \pi$ and define the path integral

$$J = \int_C \left\{ \frac{1}{2}\left[\left(\frac{\partial T}{\partial y}\right)^2 - \left(\frac{\partial T}{\partial x}\right)^2\right] dy + \frac{\partial T}{\partial x}\frac{\partial T}{\partial y} dx \right\} \quad (7)$$

where C is any contour which begins on $y = 0, x > 0$, encircles the origin ($r = 0$) in a counterclockwise sense and terminates on $y = 0, x < 0$. The value of this integral is independent of the path C along which it is evaluated [12]. This can be shown by constructing a closed path consisting of two concentric arcs $0 < \theta < \pi$ with $r = r_1, r_2$ connected by two line segments along the x-axis: $r_1 < r < r_2$ on $\theta = 0$ and π. Using Green's theorem to evaluate the integral in equation (7) over this closed contour leads to the conclusion that J is independent of the path C since the integral vanishes on the two segments along the x-axis. Furthermore, $J = 0$ in the absence of a flux singularity within the region bounded by C and $y = 0$.

If J is evaluated along a semi-circular path around $r = 0$ with a vanishingly small radius so that equation (3) dominates the terms in the integrand of equation (7), it can be shown that

$$J = J_0 = \frac{\pi}{8} A_0^2 \quad (8)$$

†This integral is derived directly from an analogy with linear-elastic fracture mechanics under antiplane strain (Mode III) conditions [12]. With $u_z(x\,y)$ denoting the out-of-plane displacement in an isotropic linear-elastic solid, the analogy follows with the shear modulus $G = 1$, $u_z \to T$, $u_{z,x} = \gamma_{zx} = \sigma_{zx} \to T_{,x}$, and $u_{z,y} = \gamma_{zy} = \sigma_{zy} \to T_{,y}$ where γ denotes strain and σ stress.

where use has been made of the asymptotic relations

$$T_{,x} = -\frac{1}{2}(A_0/\sqrt{r})\sin(\theta/2)$$

$$T_{,y} = \frac{1}{2}(A_0/\sqrt{r})\cos(\theta/2).$$

Given a numerical solution for $T(x, y)$ for a particular geometry and far-field boundary conditions, an estimate of $J = J_\infty$ can be obtained along a contour C that is far away from the singularity. Even with a relatively coarse mesh around $r = 0$, the numerical solution in an annular region that is far from the singularity where gradients are shallow is relatively accurate, so that the integration of equation (7) along a path in this region leads to an accurate estimate $J = J_\infty$. This is demonstrated in the numerical example presented below.

3. A NUMERICAL EXAMPLE

To illustrate the analyses discussed in the previous section, consider a square plate of unit dimension and unit thermal conductivity with mixed thermal boundary conditions as shown in Fig. 2. From equation (4) with $\alpha = \pi$, the point $x = 0$, $y = 0$ is a point of flux singularity while the flux is bounded at the points $(x, y) = (\pm 1/2, 1)$ and the point $(1/2, 0)$ because at these points the wedge angle $\alpha = \pi/2$. The steady temperature in the plate is governed by Laplace's equation and the conditions

$$T(x,0) = 0, \qquad 0 < x < \frac{1}{2} \quad (9a)$$

$$\frac{\partial T}{\partial y}(x,0) = 0, \qquad \frac{-1}{2} < x < 0 \quad (9b)$$

$$T(x,1) = 1, \qquad \frac{\partial T}{\partial x}\left(\pm\frac{1}{2}, y\right) = 0. \quad (9c,d)$$

From equations (3) and (5) the local behaviors of temperature and heat flux near the origin, $r \to 0$, are

$$T(r,\theta) = A_0 r^{1/2}\sin(\theta/2) \quad (10)$$

$$q_\theta(r,\theta) = -1/2A_0 r^{-1/2}\cos(\theta/2). \quad (11)$$

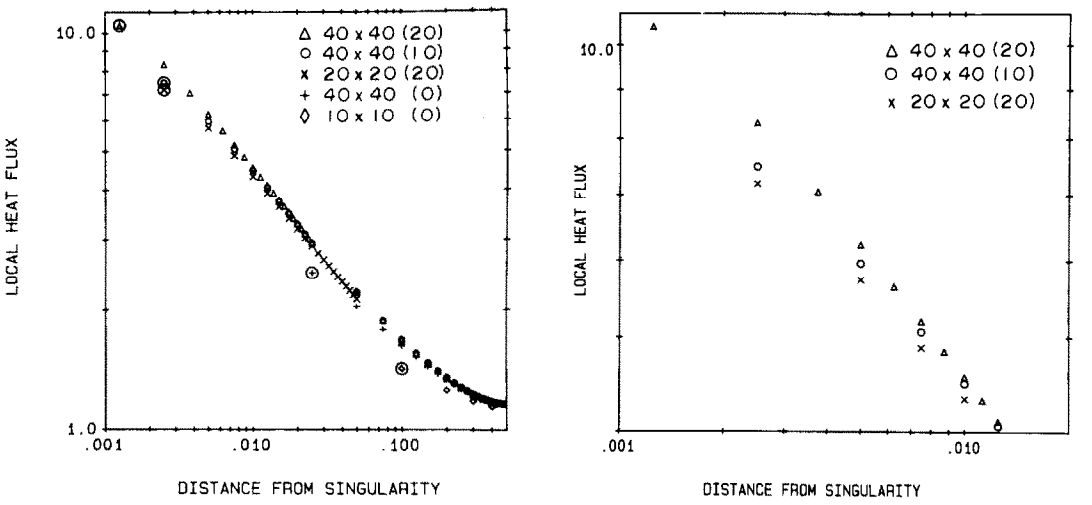

FIG. 3. Variation of local heat flux on the lower plate surface, $\partial T(x,0)/\partial y$, with distance from the singularity, x, for various mesh sizes. Data points nearest to the singularity for each mesh size are circled.

3.1. *Finite difference solutions*

Numerical solutions for conditions (9) were obtained by a finite difference technique. Central differencing was used in conjunction with a highly refined mesh in the vicinity of the origin. That is, a dense mesh is used in the space between the origin and the first outer grid lines to the left, to the right and above the origin. In discussing mesh size, the notation $N \times N(M)$ will be adopted where N is the number of grid spaces in both the x- and y-directions for the outer mesh and M is the number of grid spaces between two adjacent outer grid lines for the inner mesh. The solution was obtained for several different mesh sizes: $10 \times 10(0)$, $20 \times 20(0)$, $40 \times 40(0)$, $20 \times 20(20)$, $40 \times 40(10)$ and $40 \times 40(20)$. The $40 \times 40(20)$ mesh has 4740 mesh points, 861 of which are in the region $|x| \leqslant 0.025$, $y \leqslant 0.025$.

In Fig. 3 the flux $-\partial T(x,0)/\partial y$ for $x > 0$ obtained from the finite difference solutions is plotted vs distance from the singularity for each mesh. For each mesh, the solution at the grid line closest to the singularity is circled. Far from the singularity, $r \gtrsim 0.3$, all five meshes are in good agreement. However, near the singularity, $r \lesssim 0.1$, the uniform mesh ($10 \times 10(0)$ and $40 \times 40(0)$) results begin to deviate significantly. Very close to the singularity, e.g. $r \lesssim 0.01$, even the relatively accurate non-uniform mesh results (Fig. 3(b)) display discrepancies that significantly affect the predicted overall heat transfer as discussed below.

In heat transfer, global energy conservation is often used as a check for satisfactory convergence of a numerical solution. The heat transfer across the lower surface of the plate, with $k = 1$, is

$$Q_L = \int_0^{1/2} \frac{\partial T}{\partial y}(x,0)\,dx \tag{12}$$

Table 1. Comparison of Q_U and Q_L with and without use of the asymptotic solution

Mesh	Q_U	Without asymptotic behavior		With asymptotic behavior	
		Q_L	$\frlvert\frac{Q_L - Q_U}{Q_U}\frrvert$	Q_L	$\frlvert\frac{Q_L - Q_U}{Q_U}\frrvert$
$10 \times 10(0)$	0.843	0.677	0.197	0.766	0.091
$20 \times 20(0)$	0.831	0.713	0.142	0.786	0.054
$40 \times 40(0)$	0.826	0.742	0.102	0.800	0.032
$20 \times 20(20)$	0.824	0.782	0.051	0.805	0.023
$40 \times 40(10)$	0.820	0.793	0.033	0.813	0.009
$40 \times 40(20)$	0.820	0.799	0.026	0.814	0.007

and across the upper surface of the plate is

$$Q_U = \int_{-1/2}^{1/2} \frac{\partial T}{\partial y}(x,1)\,dx. \tag{13}$$

Comparisons of calculated values of Q_L and Q_U are given in Table 1 for the six meshes; two sets of results are tabulated. In the first set, the finite difference solutions on $0 < x \leqslant 1/2$, $y = 0$, without the asymptotic behavior analytically included, are integrated using Simpson's rule to obtain an estimate for Q_L. For the coarse $10 \times 10(0)$ mesh, heat transfer across the lower boundary is 20% below the heat transfer across the upper boundary; for the $40 \times 40(20)$ mesh it is 3% below. Since Q_U and Q_L are the overall (integrated) heat transfer, a 3% discrepancy for such a refined mesh is rather large. The second set of results (last two columns) incorporate contributions to Q_L around $x = 0$ that result from a direct integration of $\partial T(x,0)/\partial y = (1/2)A_0 x^{-1/2}$, where A_0 is determined from the J-integral as discussed below. Clearly, piecing together the asymptotic behavior with the finite difference results significantly improves the numerical solution.

Table 2. A_0 from $q_\theta(r,0)$ for $40 \times 40(20)$ mesh

r	A_0
0.00125	0.740
0.0025	0.831
0.005	0.881
0.0075	0.899
0.01	0.910
0.0125	0.917
0.015	0.922
0.0175	0.926
0.02	0.929
0.0225	0.930
0.025	0.929
0.05	0.989
0.075	1.026
0.1	1.062

3.2. *Numerical determination of* A_0

The results summarized in Fig. 3 and Table 1 demonstrate that it is difficult to determine the heat flux near $r = 0$ and even the overall heat transfer directly from the finite difference solutions. On the other hand, the complete spatial solution near $r = 0$ can be accurately described by equations (10) and (11) with an accurate estimate of A_0. On $y = 0$, with $x < 0$ adiabatic and $x > 0$ isothermal a large heat flux must be maintained along $x > 0$. Therefore, one would expect that numerically determined values of $q_\theta(r,0)$ near $r = 0$ (but not too near) should provide good data from which to estimate A_0. This is not the case as clearly seen in Table 2.

In this table, calculated values of $A_0 = -2r^{1/2} q_\theta(r,0)$ are tabulated from numerical values of q_θ in the region $0 < r \leqslant 0.1$ for the fine $40 \times 40(20)$ mesh (4740 mesh points). The fact that these estimates of A_0 vary continuously with r demonstrates that the finite difference solutions cannot accurately reproduce the $q_\theta \propto r^{-1/2}$ behavior near $r = 0$ and, therefore, that choosing an accurate value of A_0 directly from the numerical results is rather difficult. The value of A_0 calculated for this mesh using the J-integral is 0.923. Attempts to estimate A_0 from point values of either T or q showed similar and often worse trends. Coarser meshes displayed even greater variations. On the other hand, for each mesh a rather accurate estimate of A_0 is obtained from the J-integral.

To determine the strength of the singularity from equation (8), the value of J was computed from the finite difference results for six rectangular paths C around $x = 0$, $y = 0$. The right and left vertical segments of each path lie along $x = x_0$ and $-x_0$, respectively, while the upper horizontal segment lies along $y = y_0$. The calculated values of J and A_0 along the six paths for three meshes are shown in Table 3. Note that differences in J from path to path are less than 2% for the coarsest mesh and less than a fraction of a percent for the non-uniform meshes. Table 4 shows the effect of mesh size on the computed values of J and A_0 based on six paths. Note that the difference in $(A_0)_{avg}$ between the coarsest uniform mesh ($10 \times 10(0)$) and the finest non-uniform mesh ($40 \times 40(20)$) is less than 3%. The success in determining A_0 from the J-integral is due to two important properties of J: (i) since J is path independent it can be evaluated on a contour C that is chosen far from the singularity where the finite difference results are relatively accurate and (ii) since J is an integral of flux quantities it tends to smooth variations in the flux. In fact, so long as the integration path remains outside of two or three mesh spaces nearest the singularity, the variation in J is less than 5%. For example, the rectangular path with $x_0 = 0.01$, $y_0 = 0.02$ yields $A_0 = 0.914$ for the $40 \times 40(20)$ mesh which differs from the value $A_0 = 0.923$ in Table 4 by less than 1%.

Table 3. J and A_0 for several paths and mesh sizes

		$10 \times 10(0)$		$20 \times 20(20)$		$40 \times 40(20)$	
x_0	y_0	J	A_0	J	A_0	J	A_0
0.50	1.00	0.3180	0.8999	0.3314	0.9186	0.3343	0.9227
0.40	0.80	0.3174	0.8990	0.3312	0.9184	0.3343	0.9226
0.40	0.40	0.3151	0.8958	0.3306	0.9176	0.3342	0.9225
0.30	0.60	0.3169	0.8983	0.3311	0.9182	0.3342	0.9226
0.20	0.40	0.3161	0.8972	0.3310	0.9180	0.3342	0.9226
0.10	0.40	0.3128	0.8925	0.3306	0.9175	0.3343	0.9227

Table 4. J and A_0 averaged over all paths

Mesh	J_{avg}	$(A_0)_{avg}$
$10 \times 10(0)$	0.315	0.896
$20 \times 20(0)$	0.326	0.911
$40 \times 40(0)$	0.330	0.917
$20 \times 20(20)$	0.331	0.918
$40 \times 40(10)$	0.334	0.922
$40 \times 40(20)$	0.334	0.923

The discrete data in Fig. 3 is replotted as smooth curves in Fig. 4 along with the asymptotic result of equation (11) using the value $A_0 = 0.923$ obtained from the J-integral on a $40 \times 40(20)$ mesh (see Table 4). From that figure, it is clear that the overlap region for the asymptotic behavior and the numerical solutions is relatively small even for the $40 \times 40(20)$ mesh where it is approximately $0.01 \lesssim r \lesssim 0.03$. Therefore, it would be rather difficult to determine A_0 accurately via a direct asymptotic/numerical matching. An even finer mesh would be required to increase the size of the overlap region. The power and advantage of the J-integral technique is made quite clear in this context. The calculated values of Q_L labeled 'with asymptotic behavior' in Table 1 are based upon the analytical representation (11) for $\partial T(x,0)/\partial y$ near $x = 0$ with $A_0 = (A_0)_{avg}$ for each mesh. This asymptotic behavior is matched to the numerical results and then the composite solution is integrated to give Q_L. With this procedure the relative error between Q_L and Q_U is reduced by a factor of 2 for the coarsest mesh and a factor of 4 for the finest mesh.

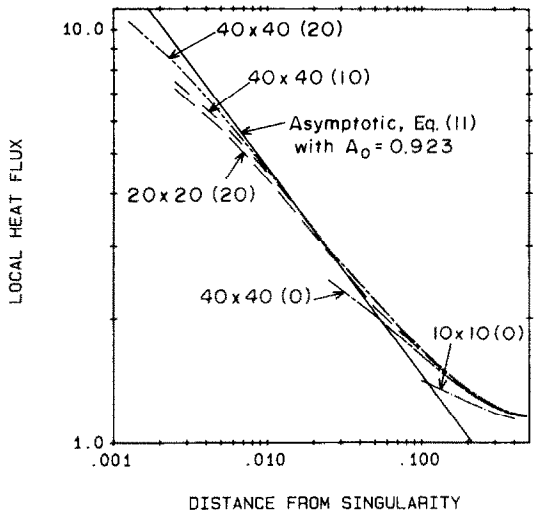

FIG. 4. Comparisons of numerical and asymptotic heat flux distribution.

The variation in Q_L with mesh refinement can be further explained by noting, from equation (11) in integrated form and Tables 1 and 4, that on $y = 0$ near $x = 0$, $-Q_\theta/Q_L \simeq 1.1x^{1/2}$. Therefore, on $y = 0$ the heat transfer along $0 \leqslant x \leqslant 0.01$ accounts for over 10% of the total heat transfer along $0 \leqslant x \leqslant 1/2$.

Finally, a simple, two-term approximation for $q_y(x,0)$ is obtained by matching the singular solution of equation (11) with the nearly constant value q_0 near $x = 1/2$. The matching point is $x^* = (A_0/2q_0)^2$. From the numerical results summarized above, $A_0 = 0.923$ and $q_0 = -q_y(1/2,0) \simeq 1.16$, so that $x^* = 0.158$. Integration of this two-term, composite approximation from $x = 0$ to 1/2 gives an estimate for $Q_L = 0.764$ which is only 6% below the best numerical value given in Table 1 (i.e. for the $40 \times 40(20)$ mesh with the asymptotic behavior analytically integrated).

4. CONCLUSIONS

Mixed boundary conditions of the isothermal–adiabatic type can result in singular behavior in flux quantities under certain circumstances ($\alpha > \pi/2$). In general, proper treatment of problems involving these singularities must combine the asymptotic solution in the nearfield, with numerical information in the farfield. The strength of the singularity A_0 can be determined approximately through an asymptotic/numerical matching process. In the special but not uncommon case of a flux singularity on a smooth boundary ($\alpha = \pi$), the strength of the singular field, A_0, is directly related to a path-independent integral which can be computed to high precision using numerical results generated on a rather course mesh. Proper treatment and use of the asymptotic behavior was shown to improve global energy conservation substantially, perhaps making extremely fine meshes unnecessary.

Acknowledgment–Discussions with D. E. Hawk and the support (for John L. Bassani) of the NSF/MRL program at the University of Pennsylvania under Grant No. 8-216718 are gratefully acknowledged. Also the authors wish to thank the National Science Foundation for its support of M. W. Nansteel and M. November under Grant Nos. MEA 83-15337 and MEA 84-14322.

REFERENCES

1. I. Sneddon, *Mixed Boundary Value Problems in Potential Theory*. North-Holland, Amsterdam (1966).
2. F. Erdogan, Mixed boundary value problems in mechanics. In *Mechanics Today* (Edited by S. Nemat-Nasser), Vol. 4, pp. 1–86 (1978).
3. J. R. Rice, Mathematical analysis in the mechanics of fracture. In *Fracture* (Edited by H. Leibowitz), Vol. II. Academic Press, New York (1968).
4. D. C. Drucker and J. R. Rice, Plastic deformation in brittle and ductile fracture, *Engng Fracture Mech.* **1**, 577–602 (1970).
5. G. E. Schneider, An investigation into the heat loss characteristics of buried pipes, *J. Heat Transfer* **107**, 696–699 (1985).
6. C. L. Tien and L. S. Yao, Analysis of conduction-controlled rewetting of a vertical surface, *J. Heat Transfer* **97**, 161–165 (1975).
7. S. S. Sadhal, Unsteady heat flow between solids with partially contacting interface, *J. Heat Transfer* **103**, 32–35 (1981).
8. S. C. Huang, Unsteady heat conduction in semi-infinite regions with mixed-type boundary conditions, *J. Heat Transfer* **107**, 489–491 (1985).
9. L. A. Clomburg, Jr., Convection in an enclosure-source and sink located along a horizontal boundary, *J. Heat Transfer* **100**, 205–211 (1978).
10. S. C. Huang and Y. P. Chang, Anisotropic heat conduction with mixed boundary conditions, *J. Heat Transfer* **106**, 646–648 (1984).
11. M. W. Nansteel, S. S. Sadhal and P. S. Ayyaswamy, Discontinuous boundary temperatures in heat transfer theory, *Int. J. Heat Fluid Flow*, under review.
12. J. R. Rice, A path independent integral and the approximate analysis of strain concentration by notches and cracks, *J. Appl. Mech.* **35**, 379–385 (1968).
13. P. Tong and T. H. H. Pian, On the convergence of the finite element method for problems with singularity, *Int. J. Solids Structures* **9**, 313–321 (1972).
14. R. S. Barsoum, Triangular quarter-point elements as elastic and perfectly-plastic crack tip elements, *Int. J. Num. Meth. Engng* **11**, 85–98 (1977).
15. L. M. Milne-Thomson, *Antiplane Elastic Systems*. Academic Press, New York (1962).
16. J. W. Hutchinson, *Nonlinear Fracture Mechanics*, Chaps 8–11, 13. Technical University of Denmark, Lyngby (1979).

CONDITIONS AUX LIMITES MIXTES ADIABATIQUE–ISOTHERME POUR LE TRANSFERT DE CHALEUR

Résumé—Des conditions aux limites mixtes de type adiabatique–isotherme sont fréquentes dans la modélisation mathématique des phénomènes de transfert thermique. Dans certaines circonstances, la condition mixte donne lieu à un comportement singulier qui ne peut être correctement traité par des moyens numériques seuls. La méthode numérique peut être complétée par une analyse asymptotique pour le comportement local proche de la singularité. Dans le cas spécial d'une condition mixte sur une frontière rectiligne, l'intensité de la singularité est donnée en fonction d'une intégrale indépendante du parcours dont la valeur peut être déterminée à partir d'une solution numérique pour le comportement au loin. On discute les implications de la considération du comportement singulier dû à la condition aux limites mixtes.

ADIABAT–ISOTHERM GEMISCHTE RANDBEDINGUNGEN BEI DER WÄRMEÜBERTRAGUNG

Zusammenfassung—Gemischte Randbedingungen vom adiabat–isothermen Typ entstehen oft bei der mathematischen Modellbildung von Wärmeübertragungsphänomenen. Unter gewissen Umständen tritt durch die gemischte Bedingung singuläres Verhalten auf, welches nicht hinreichend durch numerische Mittel allein abgehandelt werden kann. Das numerische Vorgehen muß ergänzt werden durch eine asymptotische Analyse des örtlichen Verhaltens nahe bei der Singularität. In dem Spezialfall einer gemischten Randbedingung an einer geraden Berandung wird die Stärke der Singularität in Form eines wegunabhängigen Integrals angegeben. Sein Wert kann bestimmt werden aus der numerischen Lösung für große Entfernung von der Singularität. Folgerungen aus den Zusammenhängen zwischen singulärem Verhalten und der gemischten Randbedingung werden erörtert.

СМЕШАННЫЕ АДИАБАТИЧЕСКИ–ИЗОТЕРМИЧЕСКИЕ ГРАНИЧНЫЕ УСЛОВИЯ В ТЕПЛООБМЕНЕ

Аннотация—Смешанные граничные условия адиабатически–изотермического типа часто возникают при математическом моделировании явлений теплопереноса. При определенных обстоятельствах смешанные условия приводят к сингулярностям, которые нельзя адекватно рассмотреть, используя только численные методы. Численный расчет следует дополнить асимптотическим анализом локальной структуры вблизи сингулярности. В особом случае смешанных граничных условий на прямой границе порядок сингулярности выражается через интеграл, независящий от пути интегрирования, который можно определить по численному решению для дальней области. Обсуждаются возможные последствия пренебрежения сингулярностями, обусловленными смешанными граничными условиями.